



Grain growth mechanisms in ultrafine-grained steel: an electron backscatter diffraction and in situ TEM study

Laura Ahmels¹ , Ankush Kashiwar^{1,2} , Torsten Scherer^{2,3} , Christian Kübel^{2,3} , and Enrico Bruder^{1,*}

¹Division Physical Metallurgy, Materials Science Department, TU Darmstadt, Alarich-Weiss-Str. 2, 64287 Darmstadt, Germany

²Institute of Nanotechnology, Karlsruhe Institute of Technology, Hermann-von-Helmholtz Platz 1, 767344 Eggenstein, Germany

³Karlsruhe Nano Micro Facility, Karlsruhe Institute of Technology, Hermannsschlacht Platz 1, 767344 Eggenstein, Germany

Received: 21 February 2019

Accepted: 8 April 2019

Published online:

16 April 2019

© Springer Science+Business Media, LLC, part of Springer Nature 2019

ABSTRACT

In this work, the thermal stability of the strongly elongated and textured ultrafine-grained microstructure of a high-strength low-alloy steel processed by linear flow splitting is investigated. The annealing behavior is studied for α - and γ -fiber orientations, which are dominant in the rolling type texture of the material and are known for their differences in stored energy in conventionally cold rolled steels. Electron backscatter diffraction is used to assess contributions from curvature-driven boundary migration while the contribution of strain-induced migration is investigated by comparing the annealing behavior of prerecovered to non-prerecovered samples. The exact nature of the coarsening process is studied using in situ TEM heat treatments and complementary ACOM analysis. The results show that the observed preferred growth of α -fiber grains can be fully described by curvature-driven grain boundary migration and that there is no indication for the relevance of gradients in dislocation density.

Introduction

A common characteristic of most ultrafine-grained (UFG) metals is an intrinsic instability at elevated temperatures and in some cases even at room temperature [1, 2] caused by the high defect density that results from severe plastic deformation (SPD) processing [3]. To utilize the full potential of UFG materials for structural or functional applications, the microstructure and related properties have to be optimized by subsequent

annealing [4–7] and need to be stable during service. Even if limited microstructural and thus property alterations are tolerable to some extent, they need to be predictable. Understanding the active mechanisms and driving forces that promote thermally activated coarsening processes is therefore not just an interesting topic for fundamental research but also of substantial technological relevance.

UFG materials take a special role with respect to thermal stability and annealing phenomena. Being

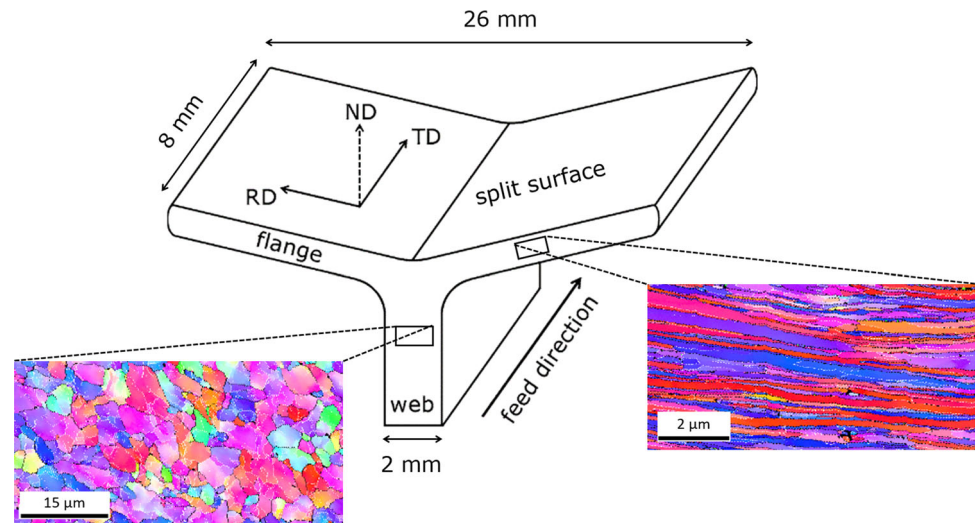
Address correspondence to E-mail: e.bruder@phm.tu-darmstadt.de

generated by severe cold working during SPD processing, they obviously qualify as deformation microstructures, yet they lack some of the key features that are typical for conventional deformation microstructures such as a variety of subgrain structures (cell walls, dense dislocation walls, microbands, etc.). This is due to the fact that the misorientation of subgrain structures increases with the imposed strain and most of them are transformed into high-angle grain boundaries (HAGBs) [1, 8]. Hence, UFG microstructures combine characteristics of deformation structures in terms of stored energy with those of recrystallized microstructures, which typically consist of a majority of HAGBs with little to no substructures. As the annealing behavior strongly depends on the deformation substructure, there have been approaches to describe the annealing behavior of UFG microstructures in terms of the fraction of substructures to the total boundary density. The role of the subgrain structure on the grain break-up during annealing was demonstrated by experiments and Monte Carlo-Potts simulations by Pragnell et al. [9]. A more quantitative approach using Humphrey's theory for the stability of cellular microstructures [10] was successfully applied to describe the transition from continuous to discontinuous coarsening during annealing of severely cold rolled aluminum as a function of the HAGB fraction and the subgrain misorientation [11]. Hence, it appears that models, which neglect driving forces from stored energy (dislocation density) in the interior of grains or subgrains, can be sufficient to capture the general annealing behavior of severely deformed metals. However, the driving forces for strain-induced boundary migration (SIBM) caused by local variations in stored energy could potentially be quite significant in UFG metals, considering that the dislocation densities after SPD processing are typically in the range of high 10^{14} m^{-2} to low 10^{15} m^{-2} [12–14]. One example that indicates a stored strain energy effect on orientation selective grain growth is the annealing behavior of UFG high-strength low-alloy (HSLA) steel processed by linear flow splitting (LFS) [15]. The material exhibits a very strong bcc rolling texture that consists of $\langle 110 \rangle \parallel \text{RD}$ (α -fiber) and $\langle 111 \rangle \parallel \text{ND}$ (γ -fiber) orientations (coordinate system see Fig. 1). During heat treatment, α -fiber grains, especially those having a $\{100\} \langle 110 \rangle$ orientation (rotated cube), show a preferred growth up to the point where they form a network of immobile

low-angle grain boundaries (LAGBs) and discontinuous growth of other orientations occurs. The pronounced orientation selective growth could be understood in terms of SIBM as the rotated cube orientation is the texture component with the lowest Taylor factor and supposedly lowest stored energy among all relevant components [16]. There are other examples for orientation selective growth in UFG materials such as the investigation on a cryo-SPD processed Al-alloy [17]. The general annealing behavior is similar to the aforementioned HSLA steel, with orientation selective growth that results in a transition from continuous to discontinuous coarsening by orientation pinning. Yet, the reason for the selective growth could not be directly related to the stored energy, since the texture components that increase during annealing belong to orientations of high stored energy (copper) as well as low stored energy (cube, goss) [18].

The present work is motivated by the insufficient knowledge on the active grain growth mechanisms during annealing of UFG metals produced by SPD. The aim is to identify the cause for orientation selective growth in an UFG material based on a detailed analysis of electron backscatter diffraction (EBSD) data as well as in situ TEM heat treatments. For this purpose, a LFS processed HSLA steel is chosen which, as mentioned before, is known for its orientation selective grain growth [15] and also offers advantages related to the LFS process. The deformation mode in the UFG region near the split surface of LFS samples (Fig. 1) is plane strain compression, which results in a very strong bcc rolling texture [15] with well-known Taylor factors for all relevant components. Due to the strength of the deformation texture, the intensities of both low and high Taylor factor orientations facilitate a statistical concept for reasonably sized EBSD maps. Quantifying the stored energy based on the Taylor factor alone is certainly an oversimplification, as the evolution of the Taylor factor during deformation is neglected [19]. Such an approach would not make any sense for SPD processes based on shear deformation such as ECAP or HPT with highly transient texture components. However, the stability of bcc rolling texture components is relatively high and there are numerous examples that confirm the validity of a qualitative correlation between Taylor factor and stored energy for cold rolled ferrite steels [16, 20].

Figure 1 Linear flow split profile with coordinate system; dimensions refer to the samples used in this work.



Despite the similarities, the LFS microstructure does not undergo primary recrystallization that is usually observed in these cold rolled steels and leads to an increase in γ -fiber area fraction [21, 22]. This is in line with Humphrey's theory as the LFS microstructure exhibits a large fraction of HAGBs inhibiting primary recrystallization [9, 11, 15, 23]. Therefore, the possible coarsening mechanisms near the flange surface of LFS profiles are SIBM and curvature-driven grain growth. While there is little doubt that curvature-driven grain growth does play a role, there certainly is a question mark behind SIBM considering the absence of substructures and the facilitated recovery in UFG microstructures. Consequently, a central aspect of this work is to find experimental proof for the presence or absence of orientation dependent variations in stored energy, by comparing the annealing behavior of prerecovered LFS profiles to profiles without thermal pretreatment.

Materials and methods

A LFS profile from HC480LA with the following chemical composition: 0.07 wt% C, 0.71 wt% Mn, 0.1 wt% Cr, 0.047 wt% Si, 0.034 wt% Nb, and 0.016 wt% Al was used, the sample geometry is shown in Fig. 1. Details on the process and processing parameters can be found elsewhere [24, 25]. Half of the used samples were subjected to a recovery annealing procedure in a furnace at 375 °C for 10 h. Then, pairs containing one prerecovered and one non-heat treated sample were simultaneously

subjected to heat treatments in a salt bath furnace at 600 °C with varying annealing times. After 10 s, 20 s, 30 s, 60 s, 90 s, 120 s, 180 s, 300 s, 600 s, 720 s as well as 900 s one of the pairs was removed from the salt bath and water-quenched to room temperature. One pair of samples was not subjected to any salt bath annealing and used as references. For microstructural analysis, the samples were ground and polished down to 0.25 μm diamond suspension, and the final polishing step was performed using OPS suspension for 5 min. EBSD measurements were carried out using a TESCAN MIRA3-XM SEM equipped with an EDAX TSL DigiView EBSD system. They were performed on a cross section (RD-ND-plane) of the samples with the center of the measured area being 50 μm below the split surface. The step size was chosen to be 20 nm with a covered area of at least 450 μm^2 containing a minimum of 500 grains (typically 2000–3000 grains at low annealing times).

All EBSD measurements were analyzed using the TSL OIM Analysis software. The cleanup routines Grain CI Standardization and Grain Dilation (single iteration) were performed on all datasets. Only points with a confidence index exceeding 0.1 were considered in the evaluation. Grains were defined with a minimum misorientation of 10° the minimum grain size was set to be 5 pixels, and the deviation of the reconstructed boundaries from the boundary segments was defined as the step size. The comparably high minimum misorientation in the grain definition ensures that all grains are separated by mobile high-angle grain boundaries (see chapter in situ experiments); low-angle grain boundaries are treated as

subgrain structures. Grains were divided into three categories: Grains belonging to the α -fiber ($\langle 110 \rangle$ II RD with 10° tolerance), grains belonging to the γ -fiber ($\langle 111 \rangle$ II ND with 10° tolerance) and grains exhibiting orientations that do not fall into the first two categories.

For mechanical characterization, all samples were subjected to hardness measurements. At 50 μm distance to the split surface, 10 HV0.05 indents were performed on each sample (RD-ND plane) and averaged.

Additionally, in situ heat treatment experiments were conducted on a TEM lamella that was extracted from an LFS profile by FIB milling (Strata 400 S, FEI Company) at a position equivalent to the areas measured by EBSD. The RD-ND oriented lamella was analyzed by ACOM-TEM using the ASTAR system (NanoMegas) installed on a Tecnai F20 ST (FEI Company) before starting the heat treatment using an Aduro MEMS-based heating holder (ProtoChips Inc.). The lamella was heated up to 300 $^\circ\text{C}$, and then the temperature was increased in steps of 50 $^\circ\text{C}$ every 10 min. After reaching 500 $^\circ\text{C}$, i.e., after 40 min, the lamella was cooled down to room temperature and another ACOM measurement was performed. Then, the heat treatment was resumed at 500 $^\circ\text{C}$ and the temperature was increased in 25 $^\circ\text{C}/10$ min steps. Reaching 625 $^\circ\text{C}$ (after 100 min), the lamella was cooled down to 400 $^\circ\text{C}$ to perform another ACOM scan, thereby reducing further grain growth to a marginal level while avoiding the thermal distortions that occur after cooling to room temperature.

For all ACOM maps, the TEM was operated at 200 kV in microprobe STEM mode using a condenser aperture of 30 μm , extraction voltage of 4.5 kV, gun lens 3, spot size 8 and camera length 8 cm. Each map was acquired using a probe that scanned the sample with a step size of 5 nm and processed at an angle of 0.4° at each step. The ACOM maps were processed using the ASTAR software package by a template matching procedure for rapid indexing of spot diffraction patterns adopted by Rauch et al. [26]. The indexing was performed using softening loops 1, spot enhance loops 3, spot detection radius 5 and noise threshold 10 within the software. After indexing, the resulting maps were corrected for 180° ambiguity to account for the ambiguous intragranular misorientations in the crystallites that result from relative low Bragg's angle in case of the TEM spot diffraction.

Results

Ex situ experiments

The microstructure of the non-heat treated reference sample shown in Fig. 2 top left exhibits an elongated UFG structure which is characteristic for the region near the split surface of LFS processed material [15, 27]. The dark spots in the inverse pole figure (IPF) maps are non-indexed points caused by carbides. The corresponding texture is represented by the $\phi_2 = 45^\circ$ section of the orientation distribution function (ODF) and reveals a fiber texture that is characteristic for bcc rolling (Fig. 2a right). It consists of an α -fiber ($\langle 110 \rangle$ II RD) and a γ -fiber ($\langle 111 \rangle$ II ND), with the highest intensity ($52 \times$ random) at the rotated cube orientation, which is part of the α -fiber.

Annealing for 900 s at 600 $^\circ\text{C}$ results in a coarser, more equi-axed microstructure with a unimodal grain size distribution lacking signs of discontinuous growth, as shown in Fig. 2b). The corresponding $\phi_2 = 45^\circ$ section of the ODF shows an increase in α -fiber intensity to a maximum of $105 \times$ random, especially for the rotated cube orientation, and a vanishing γ -fiber, which is in line with previous investigations on linear flow split steels [15]. This change in texture during annealing without the occurrence of discontinuous growth processes such as primary recrystallization will be referred to as (orientation) selective grain growth.

The microstructure and texture of the prerecovered samples prior to salt bath heat treatment in Fig. 3 exhibit very similar features to its not prerecovered equivalent. The strongly elongated microstructure shows the same rolling type texture with a maximum intensity of $63 \times$ random, the intensity along the γ -fiber is slightly lower than without preannealing. After 900 s of annealing, the microstructure of the prerecovered sample exhibits the same features as its non-prerecovered counterpart. The IPF map shows a continuously coarsened microstructure and the $\phi_2 = 45^\circ$ section of the ODF displays an increase in α -fiber intensity and a decrease in γ -fiber intensity. The decrease in γ -fiber is less pronounced than without preannealing, whereas the maximum intensity at the rotated cube orientation is slightly higher at $134 \times$ random.

The evolution of the α - and γ -fiber area fractions with increasing annealing time quantified in Fig. 4 shows a preferred growth of α -fiber orientations, i.e.,

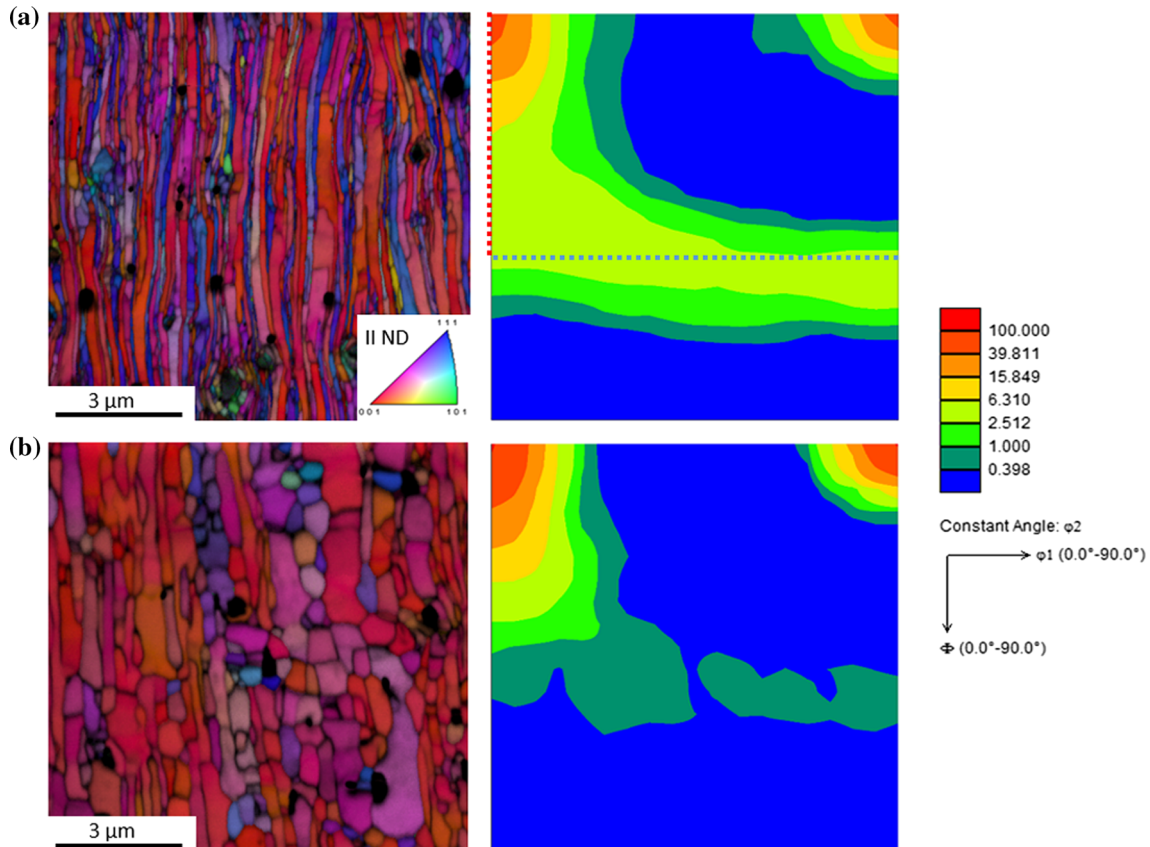


Figure 2 IPF with underlying image quality (left) and ODF $\phi_2 = 45^\circ$ section (right) of non-precovered samples **a** without salt bath heat treatment, **b** after the maximum of 900 s salt bath heat treatment at 600 °C. Red line indicates the α -fiber, and blue line marks the γ -fiber.

selective grain growth. The area fraction of the α -fiber increases from 53 to 79% in the not preannealed samples over 900 s of annealing, while the γ -fiber area fraction is reduced from 17 to 3%. The pre-covered samples display an increase in α -fiber area fraction from 58 to 74% and a decrease in γ -fiber fraction from 13 to 6% over the same period. In both cases, the grains belonging to other orientations exhibit a behavior comparable to the γ -fiber. It should be noted that both fibers overlap at $\{111\} \langle 110 \rangle$ so that the area fractions of α -fiber, γ -fiber and all other orientations do not add up to 100%.

The selective grain growth can also be observed in the evolution of the fiber grain sizes with annealing time. Due to the strong elongation of the grains as well as the strong texture (see Fig. 2), huge networks with small interconnecting areas where the misorientation is less than 10° are defined as single grains, especially in case of rotated cube oriented areas that dominate the crystallographic texture. Consequently, the grain area or average grain radius is not suitable to describe their growth. Therefore, the more

suitable inverse of the grain boundary density S_v is used to quantify the changes in grain size. In Fig. 5, it can be seen that the overall inverse grain boundary density of the not precovered samples changes from $0.14 \mu\text{m}$ at the beginning of the heat treatment to $0.93 \mu\text{m}$ after 900 s. The development of inverse grain boundary densities of the precovered samples is very similar, starting at $0.17 \mu\text{m}$ and increasing over time to a maximum of $0.9 \mu\text{m}$. In Fig. 5b, it is obvious that these changes in grain size are primarily carried by the growth of α -fiber grains from $S_v^{-1} = 0.17 \mu\text{m}$ to $S_v^{-1} = 1.27 \mu\text{m}$ in the not precovered samples and from 0.22 to $1.29 \mu\text{m}$ in the precovered case, while γ -fiber grains only exhibit minor grain growth from $S_v^{-1} = 0.1 \mu\text{m}$ to $S_v^{-1} = 0.3 \mu\text{m}$ and from 0.13 to $0.39 \mu\text{m}$, respectively. The inverse grain boundary density evolution of the grains not belonging to either α - or γ -fiber equals the behavior of the γ -fiber grains in both cases.

The strong increase in α -fiber grain size and area fraction over annealing time also influences the grain

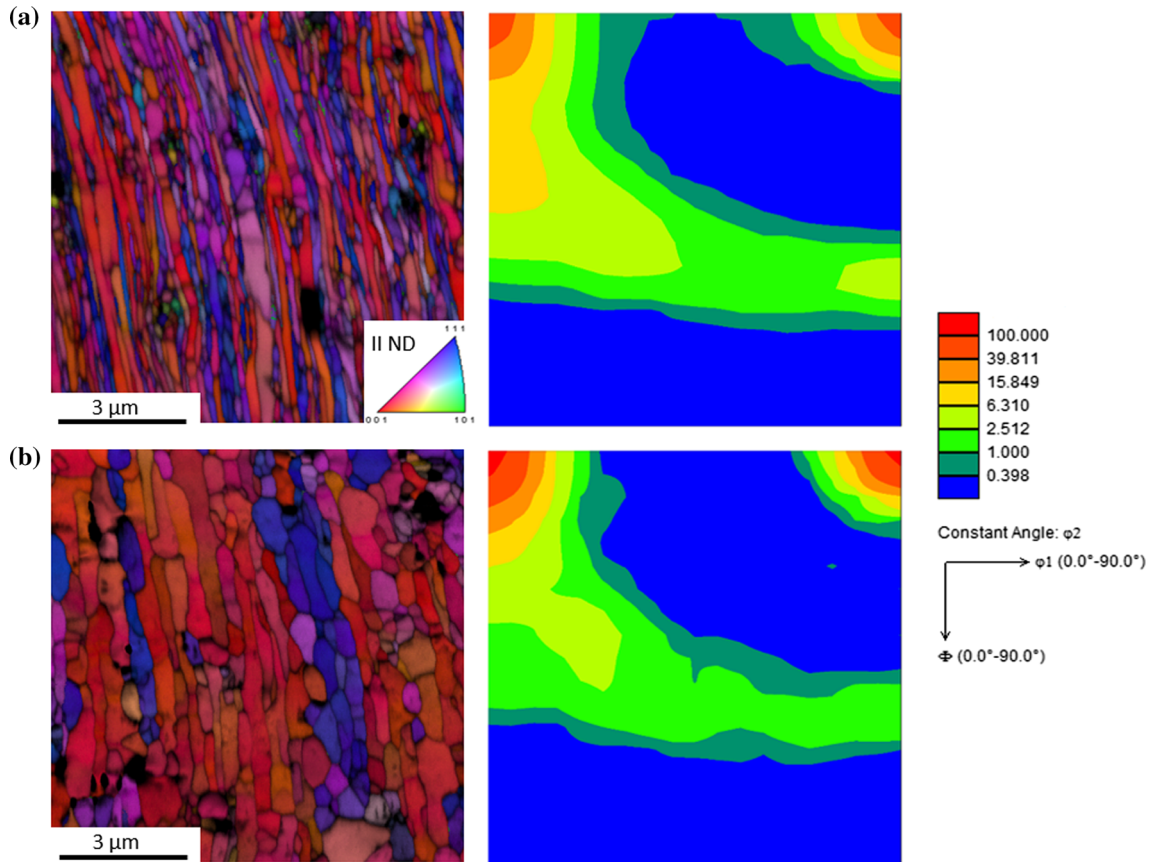


Figure 3 Microstructure and texture of prerecovered samples: **a** without salt bath heat treatment, **b** after the maximum of 900 s salt bath heat treatment at 600 °C.

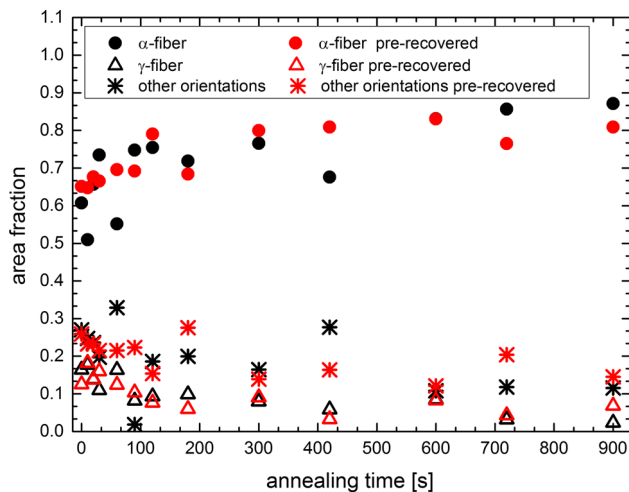


Figure 4 Area fraction of α , γ -fiber and other orientations over annealing time at 600 °C.

boundary character distribution that has a strong influence on the expected coarsening behavior. In this work, 10° is chosen as minimum misorientation for grains due to mobility reasons (see “In situ

experiments” section). To avoid confusion that might be caused by different criteria for the grain/subgrain and HAGB/LAGB distinction, 10° is also chosen to be the minimum misorientation for HAGBs. However, since the most common value in the literature is 15° , the curve considering 15° as threshold is also shown. As shown in Fig. 6, the initial HAGB fraction amounts to 72% if HAGBs are defined with a misorientation of 15° and 82% if boundaries with a misorientation higher than 10° are considered HAGBs. Over the course of annealing, this initially high value decreases to 41% ($> 15^\circ$) or 59% ($> 10^\circ$), respectively. For clarity, only the results without recovery pretreatment are displayed as the pre-recovered samples exhibit the same trend.

Since they are a measure for curvature-related driving force, the average difference in triple junctions between grains and their nearest neighbors is displayed in Fig. 7. (Exemplary distributions of this difference in triple junctions can be found in “Appendix”). Grains belonging to the α -fiber exhibit

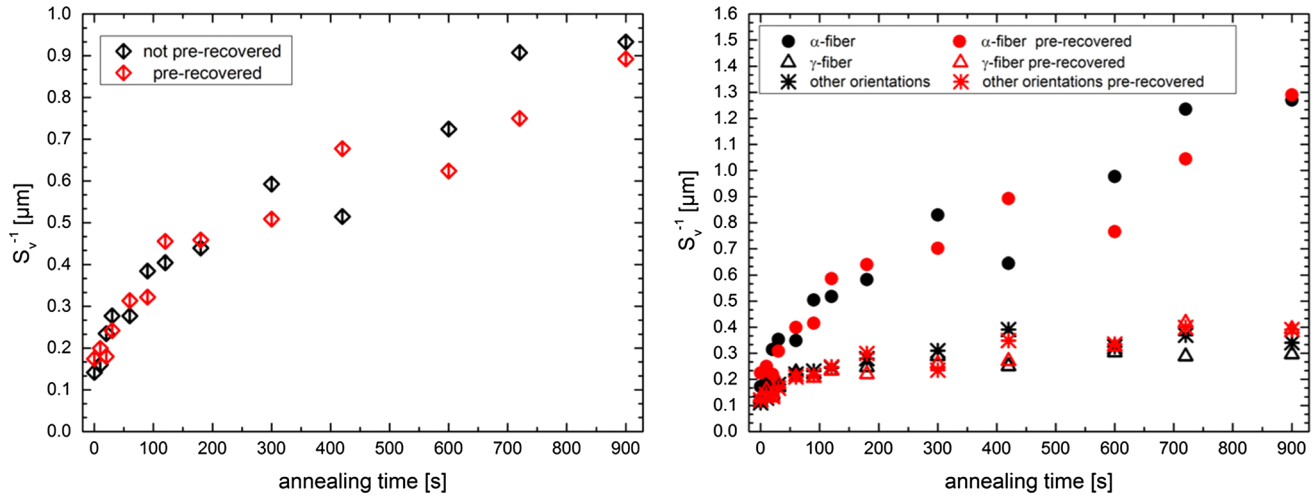


Figure 5 Inverse of the grain boundary density over annealing time at 600 °C.

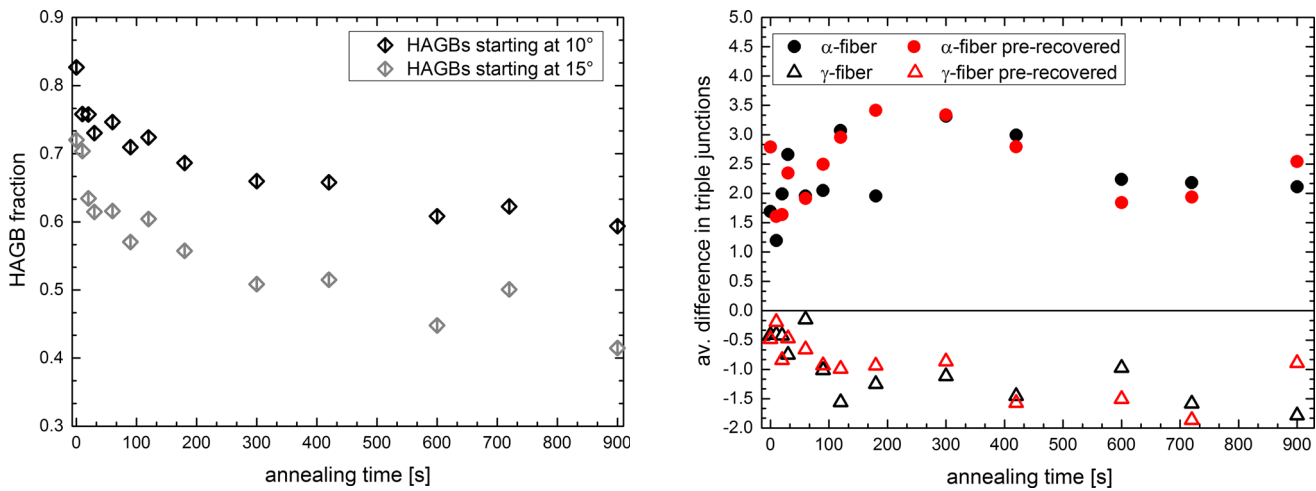


Figure 6 HAGB fraction over annealing time at 600 °C.

significantly higher values than γ -fiber grains. On average, α -fiber grains exhibit one to three triple junctions more than the surrounding grains, γ -fiber grains have on average 0.5 to 1.5 triple junctions less than their neighbors. In these plots as well as in the following, the results for grains not belonging to α - or γ -fiber will not be displayed in the interest of clarity. Their behavior has constantly be found to match the values found for the γ -fiber grains.

The change in defect density in the material during annealing can also be observed in the change in microhardness. As shown in Fig. 8, the hardness without prerecovery treatment drops from 318 HV0.05 to 230 HV0.05 after 900 s at 600 °C, with the major reduction taking place within the first 100 s of heat treatment. The prerecovery heat treatment

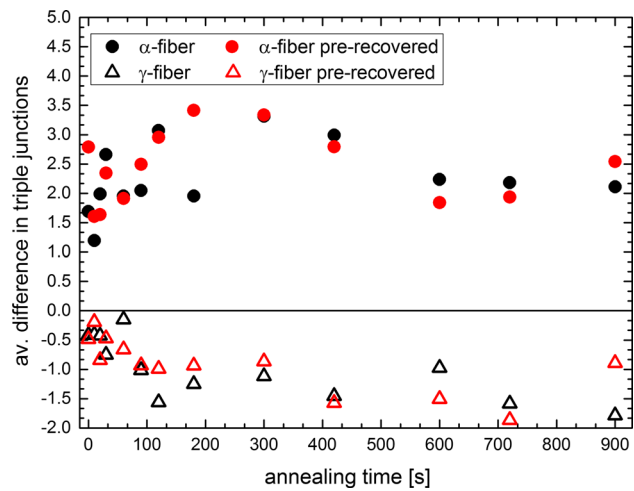


Figure 7 Average difference in number of triple junctions in comparison with the neighboring grains over annealing time at 600 °C.

reduces the initial hardness from 318 to 300 HV. In the first few seconds of annealing, however, the hardness of the preannealed samples levels with the hardness of the not pretreated samples, leading to a joint hardness curve over the course of the salt bath treatment.

In situ experiments

In Figs. 9 and 10, enlarged sections (right) of the complete IPF and IQ maps (left) of the TEM lamella at different annealing times allow a qualitative discussion of the local coarsening behavior of the material.

To give guidance and facilitate the interpretation of the maps, some stationary grains are marked with

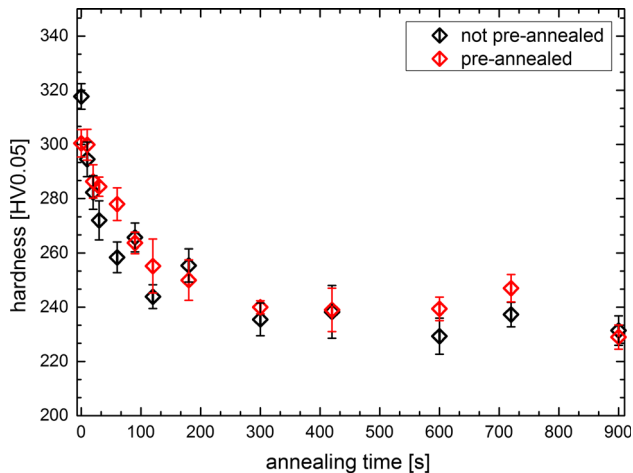


Figure 8 hardness HV0.05 over annealing time at 600 °C. Error bars indicate the standard deviation.

black numbers. White labeled grains experience significant changes in their area over the course of annealing; the migration direction of some of their triple junctions is depicted with white arrows. Looking at these arrows it is obvious that the main migration direction of the triple junctions is parallel to the pancake elongation. Mostly, thin grains decrease their length due to migration of triple junctions in elongation direction toward their lowest angle, as shown in grains #5, #7, #8 and #11. The majority of these grains belong to the γ -fiber (due to the strong texture) are surrounded by (bigger) α -fiber grains. The decrease in length of these grains therefore frequently leads to new α - α -vicinities, i.e., grains with similar orientations then neighbor each other leading to the formation of LAGBS. This can be observed for grains #1 and #2 for instance that are separated from their common neighbor by high-angle grain boundaries. After their thin, shared neighbor vanishes, the two grains end up as neighbors separated by only a very low-angle boundary. The same holds true for the grains #2 and #10 that at the beginning are separated by grain #7 and high-angle boundaries and end up divided by only a low-angle grain boundary. This way, a decrease in the HAGB fraction can be observed.

The color coding of grain boundaries in the IQ maps of the TEM lamella in Fig. 10 shows that most of the migrating grain boundaries are HAGBs with $> 10^\circ$ misorientation. The boundary #B surrounding grain #5, for example, exhibits a misorientation of 12.5° or higher and migrates significantly. However, there are some exceptions such as grain boundary #A surrounding parts of grain #1 that exhibit a

misorientation of 12.5° – 15° and a strong curvature but does not migrate. Grain #11, on the other hand, is surrounded by grain boundaries with low misorientation, partially below 7.5° that are mobile during annealing. Yet, 10° misorientation appears to be a tipping point as the majority of boundaries below 10° are immobile, while those above 10° misorientation tend to migrate in regions of pronounced curvature.

To allow a comparison with the ex situ experiments, the microstructural changes occurring in the lamella are quantified in the same manner. During the heat treatment, the area fraction of the α -fiber within the lamella increases with annealing time from 70% over 78% at 40 min to 81% after 100 min while the area fraction of the γ -fiber drops from 9% over 7% to 5%. The fraction of HAGBs decreases from 79 to 68% after 40 min and is further reduced to 59% over the course of the heat treatment.

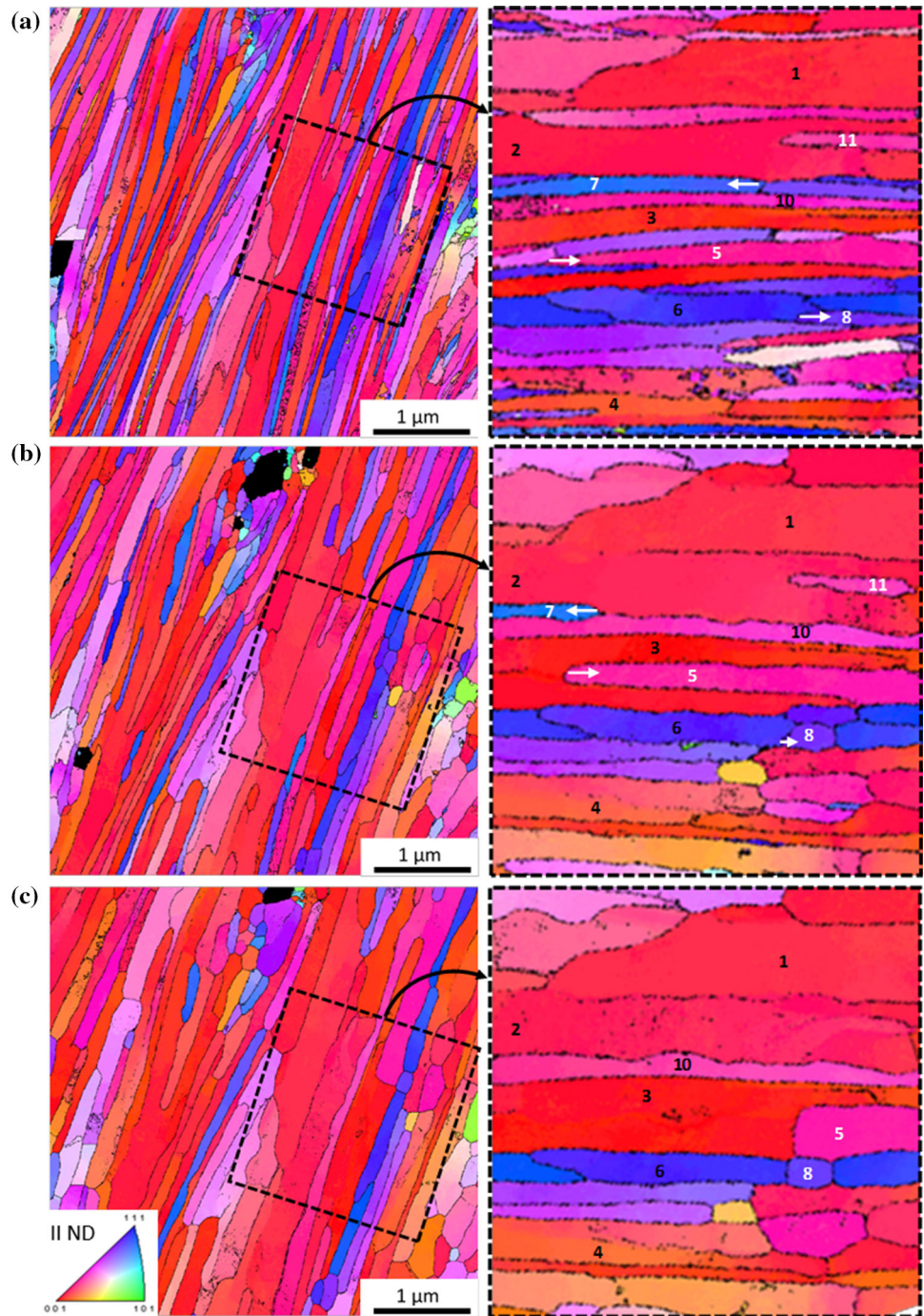
Discussion

Since the main goal of this work is to identify the underlying mechanisms causing the observed selective grain growth, the contributions of the different driving forces will be discussed separately in the following sections.

Differences in dislocation densities as driving force for selective grain growth

The dislocation density that can act as a driving force during grain growth consists of dislocations that can be stored in different places within a material: there are statistically stored dislocations randomly distributed within the grain interior or stored in low-angle substructures and geometrically necessary dislocations arranged in subgrain boundaries. The distinction between statistically stored dislocations and dislocations arranged in significant substructures is fluent and will here be made in terms of misorientation of the created structures: Dislocation substructures with resulting misorientation angle below 2° will be treated as part of the statistically stored dislocations, while dislocations organized in subgrain boundaries with a misorientation higher than 2° will be defined as geometrically necessary dislocations. The influence of dislocation densities stored at these different places on the annealing behavior will be examined in the following.

Figure 9 IPF maps of the TEM lamella during heat treatment **a** at the beginning of the heat treatment, **b** after 40 min, **c** after 100 min.



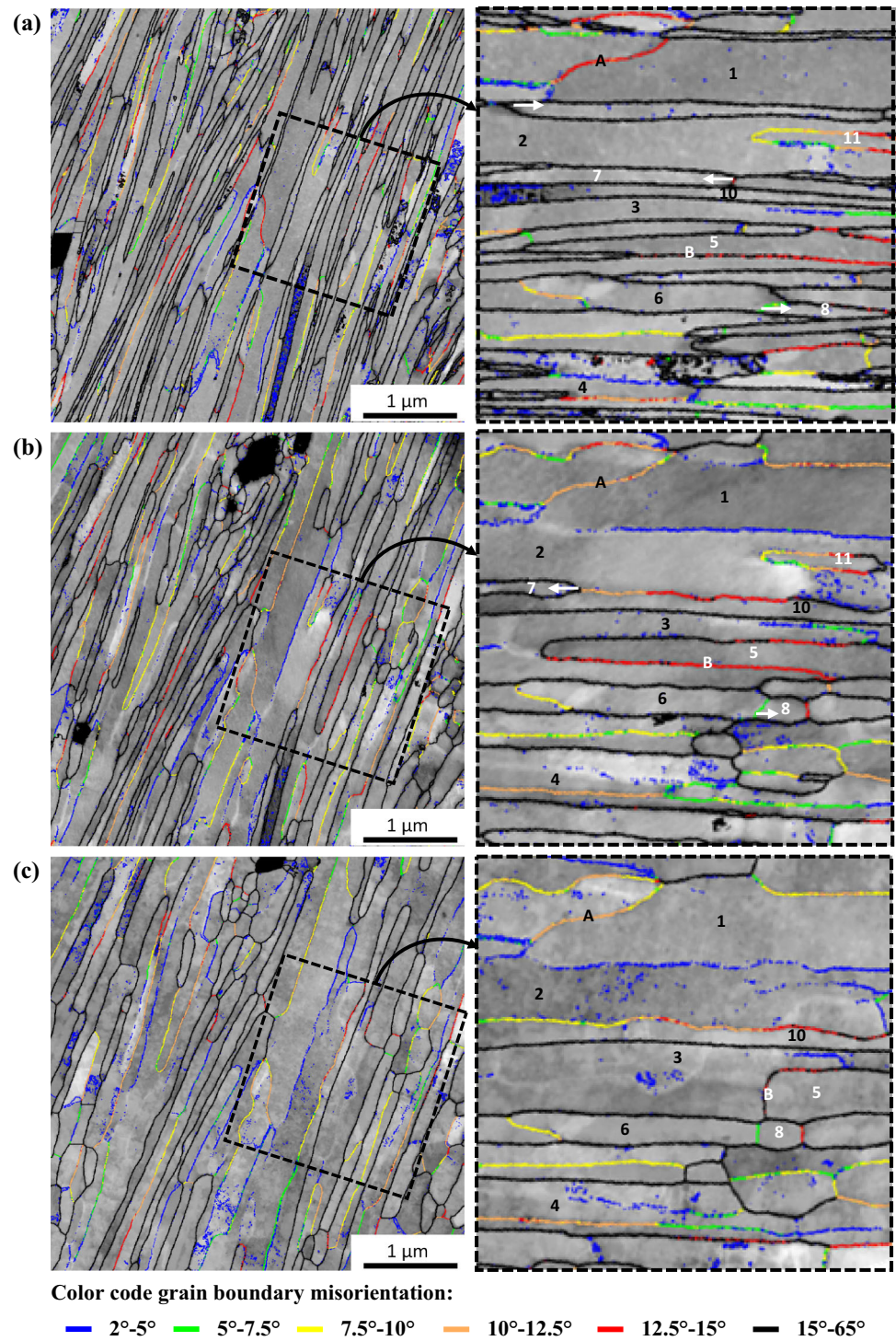
The influence of the statistically stored dislocation density can be estimated by comparing the behavior of the preannealed samples to their not preannealed counterparts.

The preannealing of the samples was shown to cause a slight increase in grain size. In a “recovery type” material with high stacking fault energy such as iron, it is known that significant recovery processes

take place before grain growth occurs [28]. Because of that, it can be assumed that the recovery treatment of the samples caused a reduction of the statistically stored dislocation density.

In the present experiments, the preceding recovery treatment, even though it affects the mechanical properties, does not influence the subsequent annealing behavior of the material as the texture and

Figure 10 IQ and grain boundary misorientation map of the TEM lamella **a** at the beginning of the heat treatment, **b** after 40 min, **c** after 100 min.



grain size evolution of the preannealed samples are equal to those found without preannealing. Therefore, the decrease in statistically stored dislocation density has no influence on the annealing behavior of the investigated material. Hence, it can be concluded that a difference in stored energy due to statistically

stored dislocations in the grain interior of the two fibers, if existing, is not a significant driving force for the selective grain growth that is observed.

In contrast to the dislocations in the grain interiors, the dislocations stored in subgrain structures such as LAGBs could have an effect on the annealing

behavior of the material. Those boundaries with low mobility might not have been affected by the recovery treatment and are a possible source for a significant driving force for grain coarsening due to gradients in stored energy. Taking into account the observations of the lamella where boundaries with $\theta < 10^\circ$ were found to be mostly immobile, these will be referred to as subgrain boundaries and will be treated as source of stored energy. In contrast, boundaries with $\theta > 10^\circ$ will be considered mobile and not be taken into account for estimating the stored energy, but will later be used to estimate the curvature-related driving force.

The dislocation density stored in subgrain boundaries can be calculated from the length of subgrain boundaries per area and their average misorientation θ . The following equation allows the calculation of the distance of dislocations D with the Burgers vector b in a subgrain boundary from its misorientation angle θ [29]:

$$\sin\left(\frac{\theta}{2}\right) = \frac{b}{2D} \tag{1}$$

Dividing the length of subgrain boundaries per area by this distance gives the number of dislocations per area, i.e., the dislocation density ρ . The stored energy E_{stored} can then be calculated from the dislocation density ρ using [28]:

$$E_{\text{stored}} \approx 0.5\rho Gb^2 \tag{2}$$

where b is the Burgers vector of iron and G is its shear modulus.

Figure 11 displaying the calculated results for the stored energy shows higher values for α -fiber grains than for γ -fiber grains for all annealing times. The initial values of α -fiber grains are in the order of 2 MPa while γ -fiber grains exhibit slightly lower values in the order of 1.7 MPa. Over the course of the annealing, the stored energy in the γ -fiber is strongly reduced while α -fiber grains show no significant change in their stored energy.

The initial difference between the fibers is caused by the strong rolling texture. The large amount of α -fiber results in a statistically high amount of α -fiber grains with similar orientations neighboring each other. Their similar orientations result in a joint boundary with low misorientation, which causes the two grains to be treated as one grain containing a substructure. This effect is most pronounced in the

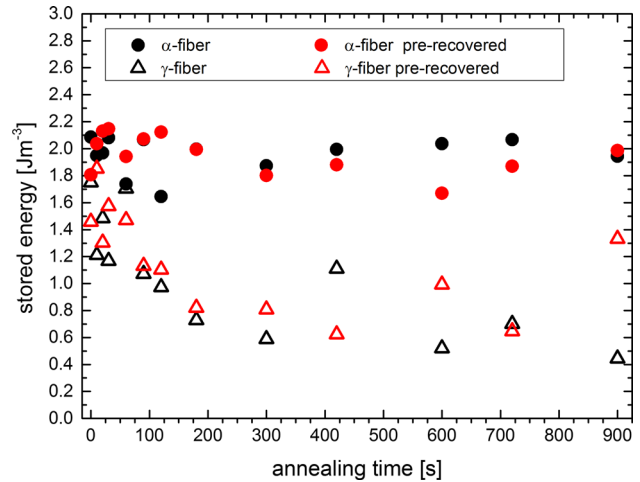


Figure 11 Estimated stored energy over annealing time at 600 °C.

rotated cube orientation that exhibits the highest predominance in the as-deformed microstructure.

However, during continuous grain growth, the growth behavior of a grain is not determined by its own stored energy, but by the difference in stored energy to its neighbors. Considering this, Fig. 11 suggests a driving force that favors the growth of the lower energy γ -fiber, which is contrary to the experimental observations. Using the initial differences in stored energy of both fibers, this driving force can be estimated to be in the order of 10^{-1} MPa. Due to the increase in stored energy differences between γ - and α -fiber over the course of the annealing, the driving force for preferred γ -fiber growth increases over annealing time.

This finding stands in strong contrast to the stored energy estimation using the Taylor factor. According to this estimation, the high Taylor factor γ -fiber should exhibit a higher dislocation density than the low Taylor factor α -fiber. Although this relation has been confirmed for conventional rolled steels [16, 20, 30, 31], there seem to be no significant dislocation density differences in the grain interiors between the two rolling texture components in the case of the LFS produced UFG microstructure. This can be explained by the fact that the grain substructures created at conventional strain ranges transform into high-angle boundaries during the high straining in LFS. This leaves only few substructures such as cell walls and dislocation walls in the microstructure after LFS. This is a key difference to conventionally rolled materials consisting of a high fraction of

substructures and explains the difference in driving forces due to grain interior dislocation density. However, the different deformation behavior of the two fibers due to the difference in their Taylor factors still has an impact on the initial microstructure: The initial grain size of the α -fiber has been found to be much higher than the γ -fiber starting grain size (see Fig. 5). This can be traced back to the higher dislocation activities in γ -fiber grains compared to α -fiber grains, causing the γ -fiber to undergo stronger grain fragmentation during the LFS process, while the α -fiber and especially rotated cube orientation with its lower Taylor factor exhibits less dislocation activity and undergoes fewer fragmentation processes. Another factor is the probability of two grains with similar orientation neighboring each other resulting in a low-angle grain boundary between them, which causes them to form a single grain. This likelihood increases with increasing dominance of an orientation or fiber in the microstructure. The given microstructure especially grains of rotated cube orientation and α -fiber grains in general exhibits an increased probability for this texture-related merging of grains, contributing to their initial grain size advantage.

Grain boundary curvature as driving force for selective grain growth

Another possible driving force for the observed selective grain growth are differences in grain boundary curvature. The curvature of a grain is influenced by its size, the character of its boundaries, and the number of its triple junctions. Whether a grain shrinks or grows can be determined purely by topological factors if a constant grain boundary energy and mobility are assumed. This assumption is reasonable, given that grains are defined as being separated by high-angle grain boundaries (minimum misorientation of 10°) in this work. A grain that exhibits less triple junctions than its neighbors is likely to exhibit a majority of convexly shaped grain boundaries, while a grain with more triple junctions than its average neighborhood is predominately surrounded by concave boundaries. Therefore, the first grain is likely to grow while the second grain with less triple junctions than its surrounding will shrink [32, 33]. Even though this approach neglects the intrinsic waviness of the grain boundaries that can be observed in Fig. 10, it can be assumed that the

contributions of these curvatures do not favor certain grain orientation dependent migration directions. Consequently, the fact that α -fiber grains always exhibit a higher number of triple junctions than their direct neighbors while γ -fiber grains have less triple junctions than their vicinity (Fig. 7) implies an advantage of α -fiber grains over γ -fiber grains in terms of curvature-related driving force for grain growth on a local scale. This advantage fits the observed increase in α -fiber area fraction and decrease in γ -fiber fraction, suggesting curvature-driven grain boundary migration to be the main coarsening mechanism here.

In the literature, a certain pattern of triple junction movement during curvature driving grain growth has been reported. In severely rolled aluminum with lamellar microstructure, triple junctions formed by three lamellar boundaries were found to migrate parallel to the grain elongation direction toward the smallest triple junction angle, leading to a shortening of thin lamellar grains [34]. This fits the observations from the TEM lamella presented in Figs. 9 and 10, where grain growth was found to be carried by the migration of these low-angle triple junctions. However, it can be argued that the coarsening mechanisms in the TEM lamella do not necessarily have to match the ex situ bulk heat treatments. The high amount of free surface and the different temperature profile that is necessary to keep the coarsening processes at an observable speed might have a substantial influence on the occurring microstructural processes. Still, the grain coarsening exhibits the same characteristics found in the ex situ experiments, an increase in α -fiber area fraction without signs of discontinuous processes. Because of that, it is assumed that the microstructural processes during the in situ and ex situ experiments are comparable. Therefore, the local coarsening mechanisms observed in the TEM lamella are likely to occur during the ex situ experiments as well. This allows the conclusion that the grain growth observed during annealing can be attributed to the curvature-related driving force, the amount of which will be estimated in the following.

The driving force for curvature-driven grain growth depends on both the grain boundary energy γ and the mean curvature radius R [28]. The von Neumann–Mullins relation [35] allows a topology based calculation of the integral curvature of a grain from the number of neighbors assuming all triple

junction angles sufficiently mobile and therefore always in their equilibrium state. Dividing this integral curvature by the perimeter of the grain results in the average curvature radius of the grain. To consider local configurations, the average difference in number of triple junctions ΔTJ of a grain to its neighbors is used instead of the difference in number of triple junctions from the topologically stable configuration with six triple junctions. Therefore, the driving force acting on a grain boundary of a grain is calculated using:

$$P_{\text{curvature}} = \frac{\pi}{3} \gamma \cdot \frac{\Delta TJ}{C} \tag{3}$$

C denotes the circumference of the grain. The grain boundary energy γ will be assumed as constant and equal to the value found for iron and therefore taken from literature: $\gamma = 1.03 \frac{\text{J}}{\text{m}^2}$ [36].

The average driving force on a grain boundary of an α -fiber grain is found to be higher than the driving force for γ -fiber grains at all regarded annealing times (Fig. 12). The driving force for curvature-driven grain growth of the α -fiber grains decreases from 0.8 to 0.5 MPa over the course of the annealing while the driving force of the γ -fiber scatters around 0.2 MPa.

Therefore, the estimated curvature-related driving force is in the same order of magnitude as the estimated driving force by stored energy. However, the grain coarsening process has been observed to be very anisotropic; as has been discussed above, the coarsening is carried by the movement of triple junctions at the tips of the grains where nearly the

complete boundary curvature is concentrated. This means that most of the boundary area of a grain is approximately stationary during grain growth, which raises doubts whether an average boundary approach is suitable for a driving force estimate. Therefore, the local driving force at the grain tips will be estimated in the following.

The main parameter influencing the local curvature radius R at the grain tips is the thickness d of the lamellar grains. The local driving force can therefore be estimated by:

$$P_{\text{curvature,tip}} = \frac{2\gamma}{R} = \gamma \frac{2\xi}{d} \tag{4}$$

ξ is a proportionality factor that is chosen to be 1 here. To determine the direction of the estimated driving force, the sign of the average difference in triple points (Fig. 7) is used. Grains with a positive average difference in triple junctions are assumed to grow, i.e., exhibit a positive driving force, while values in average difference below zero indicate shrinking due to a negative driving force.

As shown in Fig. 13, the driving force due to grain boundary curvature of α -fiber grains is positive while the γ -fiber grains exhibit negative values, consistently to the trend in their average differences in triple junctions. The amount of driving force, however, strongly decreases over the annealing time as the grains grow in thickness and the grain boundary curvature is reduced. The driving force for α -fiber grains decreases from 13 to 2 MPa, while the γ -fiber driving force increases from -17 to -6 MPa over the course of annealing. The values are of course strongly dependent on the proportionality factor ξ that is only estimated, i.e., the numbers should be treated with caution, yet, the general trends do not depend on ξ .

On this local scale, the curvature-related driving force is two orders of magnitude higher than the estimated average stored energy-related driving force; while at higher annealing times, they slowly converge to the same order of magnitude. This development in local driving force fits very well to the evolution of the fiber area fraction over time that also exhibits a strong change within the first 200 s of the annealing and levels off toward higher annealing times.

Considering these results, the selective grain growth observed in LFS profiles is plausible with regard to the higher initial grain size of the α -fiber grains that, as has been discussed before, can be

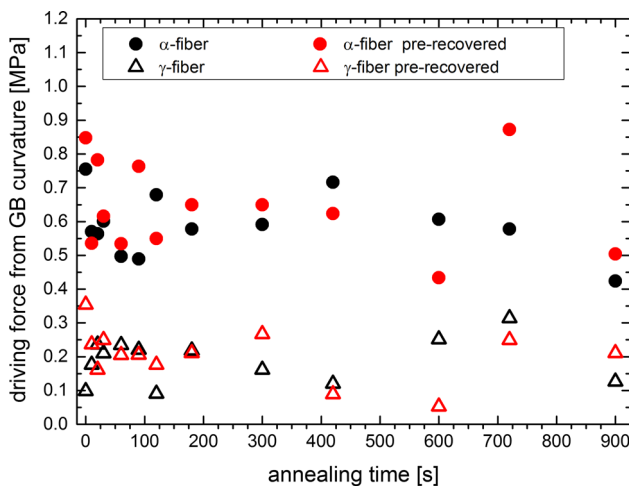


Figure 12 Average driving force from grain boundary curvature over annealing time at 600 °C.

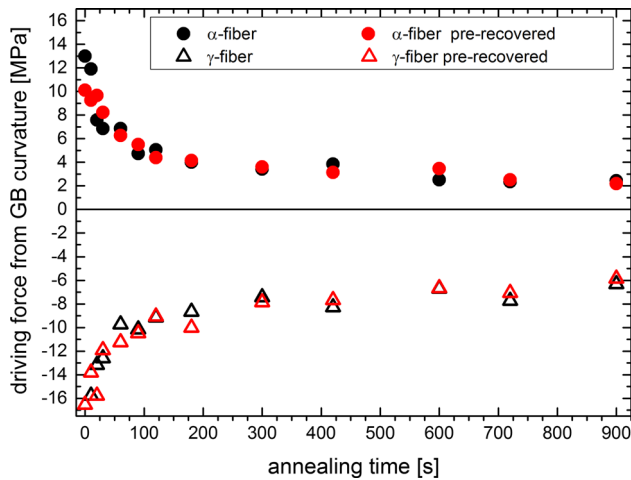


Figure 13 Local driving force from GB curvature over annealing time at 600 °C.

attributed to the lower Taylor factor of the α -fiber under plane strain compression as well as its strong predominance in the initial microstructure. The size advantage results in a higher average number of triple junctions, which implies a concave curvature of the grain boundaries to maintain the triple junction equilibrium. This leads to a driving force favoring the growth of the bigger α -fiber grains with a high number of triple junctions. Therefore, it can be concluded that the increase in α -fiber area fraction and the decrease in γ -fiber amount during annealing of the LFS material can indeed be attributed to the differences in Taylor factor between the α - and γ -fiber. However, the reason for the change in texture is not the higher Taylor factor of the γ -fiber leading to a higher dislocation density in these grains and thereby creating a stored energy-related driving force toward their shrinking and growing of α -fiber grains. Instead, the high Taylor factor leads to smaller γ -fiber grains, causing a curvature-related driving force toward their disappearance.

Overall driving force

In general, the selective grain growth can be attributed to the high curvature-related grain growth caused by the initial differences in grain size of the rolling fibers. Despite Taylor factor-based estimations, stored energy differences in the grain interiors do not influence the coarsening behavior and the energy stored in subgrain structures in the fibers favors the growth of γ -fiber grains and therefore counteracts the observed trend. Due to the high

amount of grain boundary curvature, the curvature-related driving force dominates the growth behavior of the microstructure.

However, as shown in Fig. 6 for the ex situ experiments the strong increase in α -fiber area fraction over annealing time leads to an increasing amount of LAGBs. The replacement of mobile HAGBs by less mobile LAGBs around α -fiber grains counteracts the reduction in stored energy due to the increase in grain size of the α -fiber and gives rise to an increase in stored energy-related driving force, an effect that is often referred to as orientation pinning [37–39] and can be observed in Fig. 11. This stored energy-related driving force favoring the smaller γ -fiber grains containing fewer substructures is competing with the decreasing curvature-related driving force favoring α -fiber grains displayed in Fig. 13.

At the beginning of the annealing, the driving force at the grain tips strongly favors α -fiber grains, while γ -fiber grains show a strong tendency to shrink. Over the course of the annealing, the driving forces for growth of α -fiber and shrinking of γ -fiber grains decrease. At the end of the heat treatment, small grains with a size of about 0.25 μm belonging to the γ -fiber and other orientations are surrounded by a matrix of big α -fiber grains with an inverse grain boundary density of 1.3 μm exhibiting a high amount of subgrain boundaries and nearly no driving force for grain coarsening. The small grains that are surrounded by mostly high-angle grain boundaries due to the strong texture exhibit little to no subgrain boundaries. This promotes discontinuous growth of the small grains that has also been observed in the literature [15].

Summary and conclusions

In this work, the annealing behavior of a ferrite steel subjected to severe plane strain compression via linear flow splitting is investigated. The resulting ultrafine-grained microstructure exhibits strongly elongated grains and a bcc rolling texture consisting of α - and γ -fibers. These predominant fibers are known for their pronounced differences in Taylor factor during plane strain compression.

To identify the underlying coarsening mechanisms, ex situ EBSD analyses were used to capture general and grain orientation selective trends, whereas in situ TEM investigations were used to directly observe the coarsening behavior.

- The grain refinement induced by the linear flow splitting process is more pronounced for γ -fiber orientations as compared to α -fiber orientations, which is attributed to the difference in Taylor factor between the two fibers during plane strain compression as well as the initial texture.
- The differences in grain size lead to a grain boundary curvature-related growth advantage for the α -fiber, causing an increase in texture strength of the α -fiber and especially the rotated cube component.
- A potential effect of grain orientation specific differences in the statistically stored dislocation density on the annealing behavior was not observed. Thus, strain-induced boundary migration (SIBM) is not a decisive mechanism in the early stage of annealing.
- In situ TEM investigations confirm that the main coarsening mechanism is curvature-driven boundary migration and reveal that the coarsening is predominately carried by the motion of triple junctions toward their smallest angle.
- Due to the increasing intensity of the α -fiber and especially the rotated cube orientation during annealing, the initially high fraction of HAGBs decreases due to orientation pinning.
- Orientation pinning leads to the formation of small grains surrounded by HAGBs within an α -fiber matrix with a high LAGB percentage, which is a typical starting configuration for

discontinuous coarsening that has been observed in literature.

- The occurrence of discontinuous coarsening at higher annealing times despite the high initial HAGB fraction is not captured by the unified model for grain growth. Thus, not only the initial grain boundary character distribution needs to be considered but also its change due to texture evolution during annealing, for a correct prediction of the growth behavior.

Acknowledgements

This work was carried out with the support of the Karlsruhe Nano Micro Facility (KNMF, www.knmf.kit.edu), a Helmholtz Research Infrastructure at Karlsruhe Institute of Technology (KIT). The authors gratefully acknowledge the German Research Foundation (DFG) for funding parts of this work carried out within the framework of the Collaborative Research Center 666. The funding was provided by Deutsche Forschungsgemeinschaft (Grant No. SFB666).

Appendix

See Fig. 14.

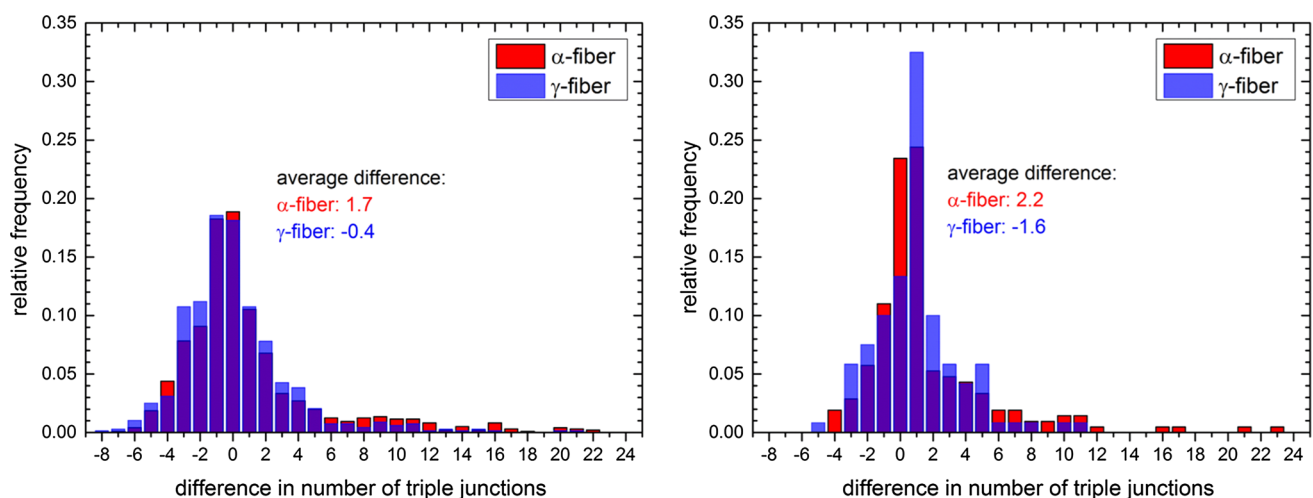


Figure 14 Distribution of the difference in number of triple junctions in comparison with the average surrounding before (left) and after 720 s (right) of annealing at 600 °C. The difference in average values between α - and γ -fiber can be attributed to the

higher frequency of α -fiber grains at high differences while the distributions are very similar around their center of gravities around zero difference.

References

- [1] Jiang H, Zhu YT, Butt DP, Alexandrov IV, Lowe TC (2000) Microstructural evolution, microhardness and thermal stability of HPT-processed Cu. *Mater Sci Eng A* 290:128–138
- [2] Wang G, Wu SD, Zuo L, Esling C, Wang ZG, Li GY (2003) Microstructure, texture, grain boundaries in recrystallization regions in pure Cu ECAE samples. *Mater Sci Eng A* 346:83–90
- [3] Čížek J, Janeček M, Srba O, Kužel R, Barnovská Z, Procházka I, Dobatkin S (2011) Evolution of defects in copper deformed by high-pressure torsion. *Acta Mater* 59:2322–2329
- [4] Hoppel H, Kautz M, Xu C, Murashkin M, Langdon T, Valiev R, Mughrabi H (2006) An overview: fatigue behaviour of ultrafine-grained metals and alloys. *Int J Fatigue* 28:1001–1010
- [5] Sergueeva AV, Stolyarov VV, Valiev RZ, Mukherjee AK (2001) Advanced mechanical properties of pure titanium with ultrafine grained structure. *Scripta Mater* 45:747–752
- [6] Park K-T, Han SY, Shin DH, Lee Y-K, Lee KJ, Lee KS (2004) Effect of heat treatment on microstructures and tensile properties of ultrafine grained C-Mn steel containing 0.34 mass% V. *ISIJ Int* 44:1057–1062
- [7] Purcek G, Saray O, Karaman I, Maier HJ (2012) High strength and high ductility of ultrafine-grained, interstitial-free steel produced by ECAE and annealing. *Metall Mater Trans A* 43:1884–1894
- [8] Pippin R, Wetscher F, Hafok M, Vorhauer A, Sabirov I (2006) The limits of refinement by severe plastic deformation. *Adv Eng Mater* 8:1046–1056
- [9] Prangnell PB, Hayes JS, Bowen JR, Apps PJ, Bate PS (2004) Continuous recrystallisation of lamellar deformation structures produced by severe deformation. *Acta Mater* 52:3193–3206
- [10] Humphreys FJ (1997) A unified theory of recovery, recrystallization and grain growth, based on the stability and growth of cellular microstructures—I. The basic model. *Acta Mater* 45:4231–4240
- [11] Jazaeri H, Humphreys FJ (2004) The transition from discontinuous to continuous recrystallization in some aluminium alloys. *Acta Mater* 52:3251–3262
- [12] Hazra SS, Gazder AA, Pereloma EV (2009) Stored energy of a severely deformed interstitial free steel. *Mater Sci Eng A* 524:158–167
- [13] May J, Dinkel M, Amberger D, Höppel HW, Göken M (2007) Mechanical properties, dislocation density and grain structure of ultrafine-grained aluminum and aluminum-magnesium alloys. *Metall Mater Trans A* 38:1941–1945
- [14] Zhao YH, Liao XZ, Jin Z, Valiev RZ, Zhu YT (2004) Microstructures and mechanical properties of ultrafine grained 7075 Al alloy processed by ECAP and their evolutions during annealing. *Acta Mater* 52:4589–4599
- [15] Bruder E (2012) The effect of deformation texture on the thermal stability of UFG HSLA steel. *J Mater Sci* 47:7751–7758. <https://doi.org/10.1007/s10853-012-6518-8>
- [16] Samajdar I, Verlinden B, van Houtte P, Vanderschueren D (1997) γ -Fibre recrystallization texture in IF-steel: an investigation on the recrystallization mechanisms. *Mater Sci Eng A* 238:343–350
- [17] Zahid GH, Huang Y, Prangnell PB (2009) Microstructure and texture evolution during annealing a cryogenic-SPD processed Al-alloy with a nanoscale lamellar HAGB grain structure. *Acta Mater* 57:3509–3521
- [18] Samajdar I, Doherty RD (1998) Cube recrystallization texture in warm deformed aluminum: understanding and prediction. *Acta Mater* 46:3145–3158
- [19] Raabe D, Hantcherli L (2005) 2D cellular automaton simulation of the recrystallization texture of an IF sheet steel under consideration of Zener pinning. *Comput Mater Sci* 34:299–313
- [20] Hutchinson B, Hansen N, van Houtte P, Juul Jensen D (1999) Deformation microstructures and textures in steels [and discussion]. *Philos Trans Math Phys Eng Sci* 357:1471–1485
- [21] Quadir MZ, Tse YY, Lam KT, Duggan BJ (2004) Rolling and recrystallization texture of cold rolled IF steel: a study from low to high deformation. *MSF* 467–470:311–316
- [22] Gong P, Sun L, Wynne BP, Palmiere EJ, Rainforth WM (2018) The effect of thermomechanical controlled processing on recrystallisation and subsequent deformation-induced ferrite transformation textures in microalloyed steels. *J Mater Sci* 53:6922–6938. <https://doi.org/10.1007/s10853-018-2029-6>
- [23] Humphreys FJ, Prangnell PB, Bowen JR, Gholinia A, Harris C, Hutchinson B, Brown LM et al (1999) Developing stable fine-grained microstructures by large strain deformation. *Philos Trans Math Phys Eng Sci* 357:1663–1681
- [24] Bohn T, Bruder E, Müller C (2008) Formation of ultrafine-grained microstructure in HSLA steel profiles by linear flow splitting. *J Mater Sci* 43:7307–7312. <https://doi.org/10.1007/s10853-008-2682-2>
- [25] Groche P, Vucic D, Jöckel M (2007) Basics of linear flow splitting. *J Mater Process Technol* 183:249–255
- [26] Rauch EF, Portillo J, Nicolopoulos S, Bultreys D, Rouvimov S, Moeck P (2010) Automated nanocrystal orientation and phase mapping in the transmission electron microscope on the basis of precession electron diffraction. *Z Kristallogr* 225:103–109

- [27] Bruder E, Bohn T, Müller C (2008) Properties of UFG HSLA steel profiles produced by linear flow splitting. *Mater Sci Forum* 584–586:661–666
- [28] Humphreys J, Hatherly M (2004) *Recrystallization and related annealing phenomena*, 2nd edn. Elsevier, Amsterdam
- [29] Lejcek P (2010) *Grain boundary segregation in metals*. Springer, Berlin
- [30] Borbély A, Driver JH, Ungár T (2000) An X-ray method for the determination of stored energies in texture components of deformed metals; application to cold worked ultra high purity iron. *Acta Mater* 48:2005–2016
- [31] Rajmohan N, Hayakawa Y, Szpunar JA, Root JH (1997) Neutron diffraction method for stored energy measurement in interstitial free steel. *Acta Mater* 45:2485–2494
- [32] Rowenhorst DJ, Lewis AC, Spanos G (2010) Three-dimensional analysis of grain topology and interface curvature in a β -titanium alloy. *Acta Mater* 58:5511–5519
- [33] Wang H, Liu GQ, Song XY, Luan JH (2011) Topology-dependent description of grain growth. *EPL* 96:38003
- [34] Yu TB, Hansen N, Huang XX (2013) Triple junction motion—a new recovery mechanism in metals deformed to large strains. *MSF* 753:485–488
- [35] Mullins WW (1956) Two-dimensional motion of idealized grain boundaries. *J Appl Phys* 27:900–904
- [36] Pelleg J (1966) On the relation between diffusion coefficients and grain boundary energy. *Phil Mag* 14:595–601
- [37] Jensen DJ (1997) Orientation aspects of growth during recrystallization. Zugl.: Lyngby-Tårbaek, Technical University, Diss., 1997, Risø National Laboratory, Roskilde
- [38] Juul Jensen D (1995) Growth rates and misorientation relationships between growing nuclei/grains and the surrounding deformed matrix during recrystallization. *Acta Metall Mater* 43:4117–4129
- [39] Engler O (1998) On the influence of orientation pinning on growth selection of recrystallisation. *Acta Mater* 46:1555–1568

Publisher's Note Springer Nature remains neutral with regard to jurisdictional claims in published maps and institutional affiliations.